Celestial Mechanics and Dynamical Astronomy (2024) 136:43
https://doi.org/10.1007/s10569-024-10202-6

ORIGINAL ARTICLE

Tidal dissipation with 3-D finite element deformation code CitcomSVE v2.1: comparisons with the semi-analytical approach, in the context of the Lunar tidal deformations

Agnès Fienga[1] · Shijie Zhong[2] · Anthony Mémin[1] · Arthur Briaud[3]

Received: 20 February 2024 / Revised: 13 June 2024 / Accepted: 14 June 2024

Abstract

Different methods are possible for estimating tidal deformations of Earth and telluric planets. On the one hand, the code ALMA^3 solves analytically the governing equations in considering symmetrical and incompressible bodies with homogeneous layers and different possible rheologies. Tidal deformations are considered with periodic excitation functions and the output of the model is frequency-dependent complex Love numbers. On the other hand, the 3-D finite element code CitcomSVE integrates numerically the governing equations with possibly lateral variations in viscoelastic structures on the regional and global scales. In this work, we present how tidal deformations have been implemented in CitcomSVE by the introduction of a periodic forcing potential. For validation and benchmarking, we realized comparisons between the ALMA^3 output for Moon tidal deformations and the numerical CitcomSVE in terms of frequency-dependent Love numbers k_2 and h_2 real and imaginary parts with 1-D viscoelastic structure. Considering two possible profiles for the Moon,we compared the frequency-dependent quality factor deduced from ALMA^3 with the one obtained with CitcomSVE. We found that with a sufficient numerical resolution for CitcomSVE (with an horizontal resolution of about 14 km and 10^{-5} for numerical accuracy), the results of the two methods for computing tidal deformations (i.e., k_2 and h_2) and quality factor Q are in good agreement for different periods including the monthly period (less than 0.025% for the real part of Love numbers and for the Q, about 1% for periods of excitation from 5 to 10^8 days). We also computed tidal dissipation energy from CitcomSVE and found it consistent

✉ Agnès Fienga
agnes.fienga@oca.eu

Shijie Zhong
shijie.zhong@colorado.edu

Anthony Mémin
anthony.memin@geoazur.unice.fr

Arthur Briaud
a.briaud@tu-berlin.de

1 Observatoire de la Côte d’Azur, Université Côte d’Azur, CNRS, IRD, Géoazur, 250 av. A. Einstein, Valbonne 06560, France

2 Department of Physics, University of Colorado Boulder, Boulder, CO, USA

3 Institute of Geodesy and Geoinformation Science, Technische Universität Berlin, 10553 Berlin, Germany

Published online: 30 September 2024

with that expected from quality factor calculation. Our study demonstrates the potential for CitcomSVE to be applied for planetary tidal deformation calculations for a planet with a 3-D structure.

Keywords Geophysics · Moon interior · Dissipation · Tides · Solid body

1 Introduction

Modeling tidal deformations can be an efficient tool for studying the internal structure of planets. For example, Briaud et al. (2023a) suggested the presence of a solid inner core of the Moon by comparing Love numbers estimated from geodetic observations with predictions from analytical models of tidal deformations. Love numbers give a description of planetary deformations (i.e., radial and tangential deformations and the perturbation of gravity potential) induced by different sources and origins (e.g., surface loadings, tides) at different spatial and timescales. Timescales range from the hour, in the case of Mars tidal deformations, to thousand of years, for the Earth glaciation and deglaciation loading. In most of the recent publications, analytical models such as ALMA^3 (Melini et al. 2022) are used for the computation of the planetary responses to the loadings and tides. ALMA^3 is very convenient and precise with different possible viscoelastic rheologies including Maxwell's but has some limitations. In particular, the analytical models assume that the planet is spherically symmetric with a layered structure, subject to the gravitational pull of a tide-raising body. However, in the solar system, indications of heterogeneities and asymmetry in planetary bodies have been well documented, mainly on temperature, density and elasticity anomalies in their mantles. For the Moon, the existence of heterogeneities in the mantle can be inferred from mare basalt volcanism and crustal thickness (e.g., Wieczorek et al. 2013). On Earth, seismic tomography studies have shown that two major anomalies called the large low shear velocity provinces (LLSVP) are present in the Earth mantle (e.g., Ritsema et al. 2011; French and Romanowicz 2015; Lau et al. 2017; Maguire et al. 2018; Duncombe 2019). For Mars, the crustal dichotomy, the Tharsis Rise and the Elysium plateau have long been viewed as evidence for heterogeneities in the mantle (e.g., Harder and Christensen 1996; Zhong 2009; Broquet and Andrews-Hanna 2023).

Calculations of deformation of a planetary body with laterally heterogeneous viscoelastic structure in response to tidal or surface forcing require special techniques including numerical (e.g., Zhong et al. 2003; Latychev et al. 2005; Klemann et al. 2008; van der Wal et al. 2013) or perturbation methods (e.g., Qin et al. 2014). However, these studies were done to account for the glacial isostatic adjustment that follows the Earth last ice age, while the studies of the lunar tidal deformation by Zhong et al. (2012) and Qin et al. (2014) only considered the effects of heterogeneous elastic structure with Heaviside function forcing time history. Tidal dissipation, and consequently tidal deformation, may play an important role in the Lunar evolution (Harada et al. 2014; Briaud et al. 2023a). Lunar tidal forcing is dominated by monthly, half-monthly and yearly periods. Therefore, it is important for the numerical models to explore tidal deformation with appropriate periodic forcings and viscoelastic mantle structure that results in dissipation.

The main objective of this work is to introduce periodic tidal excitation potentials to compute the planetary deformations of asymmetric bodies with 3-D viscoelastic structure in the open-source finite element code CitcomSVE. The paper is organized as follows. In Sect. 2.1, we present the general governing equations that describe the deformation of a planetary body under the action of a periodic potential. We present then the two methods for solving these equations: the semi-analytical approach as it is done with software such as ALMA^3 (Sect. 2.2) and the finite element method in CitcomSVE (Sect. 2.3) both for time (Sect. 2.3.1) and frequency (Sect. 2.3.2) tidal forcing functions. We also describe how the total tidal dissipation and the quality factor, Q, are computed in CitcomSVE and ALMA^3 in Sect. 2.3.3 and how they can be compared with those proposed by Efroimsky (2012). Finally, in Sect. 3, we give the results of the ALMA^3 versus CitcomSVE comparisons obtained for a 2-layered and a 4-layered Moon and conclude in Sect. 4.

2 Formulation of the tidal deformation and dissipation

2.1 The governing equations

The governing equations for planetary deformation are the laws of conservation of mass and momentum, coupled with Poisson's equation for gravitational potential. With the assumption that a planetary mantle is an incompressible medium, the equations are (e.g., Wahr et al. 2009; Zhong et al. 2022)

$$\begin{cases} u_{i,i} = 0, & (1) \\ \sigma_{ij,j} + \rho_0 \phi_{,i} - (\rho_0 g u_r)_{,i} - \rho_1^E g_i + \rho_0 V_{T,i} = 0, & (2) \\ \phi_{,ii} = -4\pi G \rho_1^E, & (3) \end{cases}$$

where u_i is the displacement with u_r being in the radial direction, ϕ is the perturbation to gravitational potential, V_T is the applied forcing potential, σ_{ij} is the stress tensor, ρ_0 is the unperturbed mantle density, g_i is the gravitational acceleration with $g = \sqrt{(g_i g_i)}$, $\rho_1^E = u_i \rho_{0,i}$ is the Eulerian density perturbation,[1] and G is the gravitational constant. The boundary conditions are zero shear and normal force at the surface (at radius $r = r_s$, Eq. (4)) and zero shear and self-gravitating normal forces at core–mantle boundary (CMB) ($r = r_b$, Eq. (5)).

$$\begin{cases} \sigma_{ij} n_j = 0, \ \text{for}\, r = r_s, & (4) \\ \sigma_{ij} n_j = (-\rho_c \phi + \rho_c g u_r) n_i, \ \text{for}\, r = r_b, & (5) \end{cases}$$

where ρ_c is the density of the core and n_i represents the normal vector of the surface or CMB. The boundary conditions at the CMB consider the self-gravitational effect for a fluid core (Zhong et al. 2003). The boundary conditions for Poisson's equation (i.e., Eq. (3)) are the continuity in the potential and its radial gradients at the surface and CMB (Zhong et al. 2003). For an incompressible mantle with a viscoelastic Maxwell rheology, the constitutive equation relating stress to strain tensors is

$$\sigma_{ij} + \frac{\eta}{\mu} \dot{\sigma}_{ij} = -P \delta_{ij} + 2\eta \dot{\epsilon}_{ij}, \qquad (6)$$

where P is the dynamic pressure, δ_{ij} is the Kronecker delta function, and μ and η are the shear modulus and viscosity, respectively, and ϵ_{ij} is the total strain tensor as a sum of elastic and viscous strains[2] and can be related to displacement u_i by $\epsilon_{ij} = (\partial u_i/\partial x_j + \partial u_j/\partial x_i)/2$. Without loss of generality, we consider, in this work, a simplified form of tidal potential

[1] An indicial notation is used here with A, i representing the derivative of variable A with respect to coordinate x_i, and repeated indices indicate summation.

[2] the dot over a variable represents time-derivative.

acting on the Moon at spherical harmonic degree $l = 2$ and order $m = 0$ and at tidal period T (Wahr et al. 2009),

$$V_T(r, \theta, t) = \frac{3eGmr_s^2}{2a^3} \left(\frac{r}{r_s}\right)^2 P_{20}(\cos\theta) \cos\left(\frac{2\pi t}{T}\right) \tag{7}$$

where r and θ are the radius and colatitude; t is the time; r_s is the Moon radius; a and e are the semi-major axis and eccentricity of the lunar orbit; m is the Earth mass; $P_{20}(\cos\theta)$ is the degree 2, order 0 Legendre polynomial. The governing equations with the boundary conditions, applied tidal potential and viscoelastic mantle structure yield solutions of displacements, strain and stress in the mantle including the surface. We are particularly interested in determining the time-dependent radial displacement and gravitational potential Love numbers h_2 and k_2 at the surface that are related to degree-2 radial displacement u_{r_2} and gravitational potential ϕ_2 at the surface by

$$\begin{cases} u_{r_2} = h_2 \dfrac{V_T}{g} & (8) \\ \phi_2 = k_2 V_T & (9) \end{cases}$$

It is interesting to note that at the surface where $r = r_S$, the potential of Eq. (7) can be written such as

$$V_T(r_S, \theta, t) = V_{T_0} P_{20}(\cos\theta) \cos\left(\frac{2\pi t}{T}\right), \tag{10}$$

where

$$V_{T_0} = \frac{3eGmr_S^2}{2a^3}. \tag{11}$$

For solving the governing equations, two approaches are possible: (i) the semi-analytical solution of the equations using Laplace transform such as with ALMA^3 (Melini et al. 2022) and (ii) the numerical method such as the finite element method used with CitcomSVE (Zhong et al. 2022). While the semi-analytical method is computationally fast, it can only be applied to a planetary body with a viscoelastic structure with spherical symmetry (i.e., 1-D). Numerical models like CitcomSVE work for a planetary body with 3-D viscoelastic structures.

2.2 The semi-analytical approach

ALMA has been developed since 2006 to estimate Earth deformations induced by surface loadings through the computation of time-dependent Love numbers (Spada and Boschi 2006; Spada 2008). Several applications of ALMA can be found in the literature. For example, it has been used to better understand Glacial Isostatic Adjustment processes (Spada 2011) or, inversely, to achieve better inferences of Earth mantle properties from geophysical observations (Boughanemi and Mémin 2024). More recently, tidal periodical deformations (without contact) and viscoelastic normal modes have been included in ALMA, leading to the ALMA^3 version (Melini et al. 2022).

Here, we only recall the main theoretical background of ALMA^3. A full description can be found in Melini et al. (2022), Briaud et al. (2023a). In all versions, ALMA computes Love numbers for an incompressible, self-gravitating, radially stratified planetary model, using as inputs multilayered 1-D rheological profiles (i.e., radius, density, shear modulus and viscosity) with homogeneous layers. See Table 1 as an example of profile.

Table 1 Parameters for 2-layered and 4-layered Moon models

		R (km)	η (Pa s)	ρ (kg m^{-3})	μ (Pa)
			2-Layers		
Mantle	Maxwell	1737.0	10^{21}	3300	6.56×10^{10}
Core	Fluid	380	–	6000	–
			4-Layers		
Crust	Maxwell	1737.0	10^{24}	3300	1.60×10^{10}
Mantle	Maxwell	1698.4386	10^{21}	3300	6.56×10^{10}
LVZ	Maxwell	500	10^{18}	3300	6.56×10^{10}
Core	Fluid	380	–	6000	–

R stands for the outer radius of each layer, η the viscosity, ρ the density and μ the shear modulus. The density and shear modulus are constant per layer. In the 2-layer case, the characteristic time scale is the Maxwell time $\tau_M = \frac{\eta}{\mu}$, which is about 484 years for mantle viscosity $\eta = 10^{21}$ Pa s and shear modulus $\mu = 6.56 \times 10^{10}$ Pa used here. The surface gravitational acceleration g_s is 1.616 m s^{-2} and the CMB gravitational acceleration g_{cmb} is 0.637 m s^{-2}

The original version of ALMA evaluates time-dependent Love numbers for a Heaviside-like forcing potential. Within the framework of viscoelastic normal modes (VNM), the computation of Love numbers is performed in the Laplace domain, followed by a numerical inverse Laplace transform to retrieve Love numbers in the time domain. Considering tidal periodic potential, ALMA^3 computes the Laplace-transformed solution of the equilibrium equations for a given harmonic degree n, leading to frequency-dependent Love number estimations. The dependency in frequency $\omega = \frac{2\pi}{T}$ corresponds to the frequency of the forcing potential, introduced here as $e^{i\omega t}$, of the fundamental equations (see Eq. (7)). If $x_\delta(t)$ is the time-domain response to an impulsive load, the solution vector, $x_\omega(t)$, for the frequency-depend forcing potential is then given by (Melini et al. 2022)

$$x_\omega(t) = x_0(\omega)e^{i\omega t}, \tag{12}$$

where $x_0(\omega)$ is the Laplace transform of $x_\delta(t)$ evaluated at $i\omega$. It is then possible to deduce Love numbers for the global gravitational response k, radial and tangential displacements (h and l, respectively) for a periodic forcing of frequency ω as direct functions of the three components of the vector $x_0(\omega)$ (see Eqs. (22, 23, 24) in Melini et al. (2022)). By design, ALMA^3 uses sequential values of ω, producing Love numbers estimated for a range of frequencies defined by the user. Furthermore, Love numbers produced here are complex numbers with a phase shift corresponding to the delay between the external periodic potential and the planet response, related to the energy dissipation within the planetary mantle. As described for example by Murray and Dermott (2000), the phase shift ϵ associated with the dissipative process is usually defined according to Love numbers such as

$$h_n(t) = \|h_n(\omega)\|e^{i(\omega t-\epsilon)} \tag{13}$$

One can then identify

$$\tan(\epsilon) = -\frac{\text{Im}(h_n(\omega))}{\text{Re}(h_n(\omega))}. \tag{14}$$

The ratio between the energy loss by dissipation and the total energy of the body is often given in terms of quality factor Q which also depends on the excitation frequency ω such as

Efroimsky (2012):

$$Q(\omega) = -\frac{\|h_n(\omega)\|}{\mathrm{Im}(h_n(\omega))} \tag{15}$$

For h_n determined from the semi-analytic method ALMA[3], such defined Q is referred to as Q_{ALMA} and when one uses the h_n deduced from CitcomSVE, Q is referred to Q_{SVE}.

2.3 CitcomSVE numerical model

CitcomSVE is an open-source finite element package for modeling deformation of a viscoelastic planetary mantle and crust in response to surface and tidal loadings (Zhong et al. 2022). This package was developed out of the mantle convection code CitcomS (Zhong et al. 2000, 2008) by replacing a viscous rheology and Eulerian grid in CitcomS with a viscoelastic rheology and Lagrangian grid (Zhong et al. 2003). CitcomSVE has been used to study glacial isostatic adjustment process and its associated sea-level change for the Earth with 3-D viscosity structure (Zhong et al. 2003; Paulson et al. 2005; A et al. 2013) and non-Newtonian viscosity (Kang et al. 2022) and also for tidal response of the Moon with 3-D elastic structure (Zhong et al. 2012; Qin et al. 2014). CitcomSVE has been demonstrated to be accurate, robust and computationally efficient with recent test calculations on more than 6000 CPU cores (Zhong et al. 2022, 2003). The package was made publicly available via github recently https://github.com/shjzhong/CitcomSVE.

With the free surface boundary conditions at the top boundary and zero shear stress and self-gravitating normal forces at the CMB (Eqs. (4) and (5)), CitcomSVE in principle works only for a single solid layer (e.g., the silicate mantle/crust for rocky planetary bodies or ice for icy satellites) of a spherical shell bounded by inviscid fluids above and below the solid layer. However, CitcomSVE may also work for a solid metallic core inside a rocky planetary bodies if the core viscosity is sufficiently smaller than that of the mantle or for two layers of ice with a fluid layer in between for icy satellites. In the latter case, CitcomSVE will need to include a layer with much smaller (e.g., several orders of magnitude) viscosity than those of the icy layers above and below. Vigorous numerical tests and benchmarks for CitcomSVE are required before it can be applied to these scenarios.

2.3.1 Time-varying deformation due to periodic tidal forcing

For a viscoelastic Maxwell medium, a characteristic timescale is the Maxwell time $\tau_M = \frac{\eta}{\mu}$, and as an example, the Maxwell time is about 484 years for mantle viscosity $\eta = 10^{21}$ Pa s and shear modulus $\mu = 6.56 \times 10^{10}$ Pa. When a tidal excitation timescale (e.g., the period T) is larger than or comparable with τ_M, mantle deformation including the surface deformation is controlled by viscous process, which is accompanied by significant viscous dissipation. On the other hand, when the tidal excitation timescale is significantly smaller than τ_M, the deformation is largely elastic. For example, in studying the effects of 3-D structure on lunar tidal deformation, because the dominant tidal period is about a month, Zhong et al. (2012) and Qin et al. (2014) only considered the elastic deformation and completely ignored viscous dissipation. However, the lunar laser ranging studies indicate a significant lunar tidal dissipation (e.g., Williams and Boggs 2015), and viscous dissipation effects have been considered in some tidal deformation calculations (e.g., Briaud et al. 2023a; Tan and Harada 2021; Harada et al. 2014). The viscous dissipation in a viscoelastic Maxwell medium affects not only the amplitude of deformation but also the phase difference between the deformation and the tidal force. The larger the viscous dissipation, the larger the phase shift ϵ, and the phase shift helps determine the tidal dissipation and tidal Q factor (see Sect. 2.2). While semi-analytical solutions have been routinely used to compute tidal Love numbers, Q and viscous dissipation in viscoelastic models (e.g., Roberts and Nimmo 2008), calculations of the phase shift and tidal Q have not been done in numerical models. In a 2-D Cartesian finite element modeling study, Devin and Zhong (2022) showed that the phase shift between the surface deformation and periodic loading force is significant for relatively large loading periods and is responsible for viscous dissipation. However, they did not quantify either the phase shift or the Q factor.

In this study, we use CitcomSVE to compute tidal deformations of the lunar mantle induced by a periodic tidal forcing (i.e., Eq. (7)) with different viscoelastic structures (for 2-layered and 4-layered Moon) and tidal periods (from 1 to 10^8 days). The surface displacement computed from CitcomSVE is used to determine the phase shift and tidal quality factor Q (i.e., Q_{SVE}) that will be compared with those determined from semi-analytical solutions provided by ALMA^3 (i.e., Q_{ALMA}).

In order to make such comparisons, we treat the lunar mantle as an incompressible medium with 1-D viscosity structure but constant density and shear modulus (see Table 1).

The accuracy of a numerical method such as CitcomSVE depends on spatial and temporal resolutions of the finite element grid. For relatively short tidal period T (i.e., comparable with or less than τ_M), we set the time increment Δt for each time step to be $\Delta t = T/N$, with N=20 or more. However, for T significantly larger than τ_M, we will generally limit Δt to be smaller than τ_M. CitcomSVE uses a non-Gauss–Legendre grid to generate a relatively uniform element size on a spherical surface and to avoid the excessive resolution near the polar regions induced by the conventional Gauss–Legendre grid. The spherical surface is first divided into 12 spherical caps with each cap as a solid angle sector of a spherical shell. Each cap is then further divided into grid cells or elements (Zhong et al. 2000). In our calculations, we employed different spatial resolution, e.g., $12 \times (32 \times 32 \times 128)$, where the last number, 128, in the parenthesis indicates the number of elements in radial direction, while the first and second numbers are for the numbers of elements in two horizontal directions. For each model calculation, CitcomSVE computes 3-D displacement, strain and stress fields on the finite element grid points and at each time step. The displacement field on the grid points is then expanded into a spherical harmonic domain in which CitcomSVE computes and outputs time-dependent surface radial displacement (h) and gravitational potential (k) Love numbers at desired spherical harmonic degrees (e.g., degree 2) (Zhong et al. 2022).

2.3.2 Frequency-dependent Love numbers and Q factor

In order to validate the implementation of the tidal forcing in CitcomSVE, we compare the obtained Love numbers with the one produced by ALMA^3 as described in Sect. 2.2. By construction, CitcomSVE computes in the time-domain displacements and gravitational potential anomalies when ALMA gives frequency-dependent Love numbers. In this work, we have chosen to transform the time-dependent CitcomSVE outputs into frequency-dependent values, comparable with ALMA^3 ones. This is a convenient approach as the user can provide the tidal frequency ω (and the corresponding period $T = \frac{2\pi}{\omega}$) as an input of the numerical code and can then fit the periodic signal (corresponding to the given ω) in the normalized radial displacement at the surface, $\bar{u}_{r_2}$ (or gravitational potential anomalies, $\bar{\phi}_2$) time series $L(t)$ provided by CitcomSVE. $\bar{u}_{r_2}$ (resp. $\bar{\phi}_2$) is related to radial displacement at the surface $u_{r_2}(t)$ (see Eq. (8)), the amplitude of periodic forcing V_{T_0} (see Eq. (11)) and gravitational acceleration at the surface g as

$$\bar{u}_{r_2}(t) = u_{r_2}(t) \times \frac{g}{V_{T_0}}$$

Note that the subscript 2 indicates degree 2, given that we only consider degree-2 tidal forcing. We have the equivalent definition for $\bar{\phi}_2$ with $\bar{\phi}_2 = \frac{\phi_2}{V_{T_0}}$. $L(t)$ stands either for $\bar{u}_{r_2}$ or $\bar{\phi}_2$. The fitted cosine and sine terms give the real and the imaginary parts of Love numbers, respectively, such as:

$$L(t) = A(\omega) \times \cos\left(\frac{2\pi t}{T}\right) + B(\omega) \times \sin\left(\frac{2\pi t}{T}\right) \tag{16}$$

where $A = A(\omega)$ and $B = B(\omega)$ lead to the real and the imaginary parts of Love numbers. The tidal phase shift is then $\epsilon = -\arctan\frac{B}{A}$ (as given by Eq. (14)) and the quality factor Q is given by $Q_{\mathrm{SVE}} = -\frac{\sqrt{A^2+B^2}}{B}$, as in Eq. (15). With the determination of A and B, it is also possible to estimate the fit uncertainties for the two terms. These uncertainties depend on the CitcomSVE numerical accuracy but also on the time resolution of the outputs. As for all least square fit, a sufficient number of points (i.e., results obtained for a given time step) is indeed required for estimating the parameters with a good accuracy (see Sect. 3.1). Experimentally, we set up this number to a minimum of 20 steps per period.

For illustration, we show, in Fig. 1, the normalized surface radial displacement $u_{r_2}(t)$ obtained with CitcomSVE for the same viscoelastic 2-layered structure (see Table 1) but with two periods of excitation: 10^4 years (Fig. 1A) and 100 years (Fig. 1B). The values of the h_2 real and imaginary parts are plotted on Fig. 2 that also shows results for other periods from 1 to 10^8 days. For each of the plots of Fig. 1, we plotted with dots the values obtained from CitcomSVE with the phase shift induced by the viscoelastic contribution of the 2-layered rheological structure and with crosses the values without phase shift. One can see, for the simulations with 10^4 year-excitation period, a very large phase shift (of about 70°), whereas for the shorter period of excitation, the phase shift is smaller (of about 2°) and almost not visible. This example illustrates why the uncertainty in computing the imaginary part of the Love number and consequently the phase shift and the energy dissipation is bigger when the period of excitation decreases. Note that for periods greater than 10^4 years, we use a time buffer of about 1.5 periods in order to reach a stable state for the solution. We have applied this method for different ranges of frequencies. The results are presented in Sects. 3.1 and 3.2.

2.3.3 Calculations of the total dissipation energy

Tidal dissipation energy for the mantle can be calculated using two different approaches. The first is based on the quality factor Q (e.g., Efroimsky 2012), and the second is from direct integration of viscous dissipation for the mantle (e.g., Devin and Zhong 2022; Hanyk et al. 2005).

Quality factor-based method The energy balance dictates that for an incompressible viscoelastic medium under external force (e.g., tidal force or surface loading) on its boundaries, the rate of work or power done at the boundaries by the external force is equal to the sum of powers of stored elastic energy and dissipative energy in the medium (Devin and Zhong 2022). For a periodic tidal forcing that is considered here, the stored elastic energy over a full loading period is zero, and the total tidal dissipation energy occurred in the planetary body is equal to the work done by the tidal force at the boundaries. According to Efroimsky

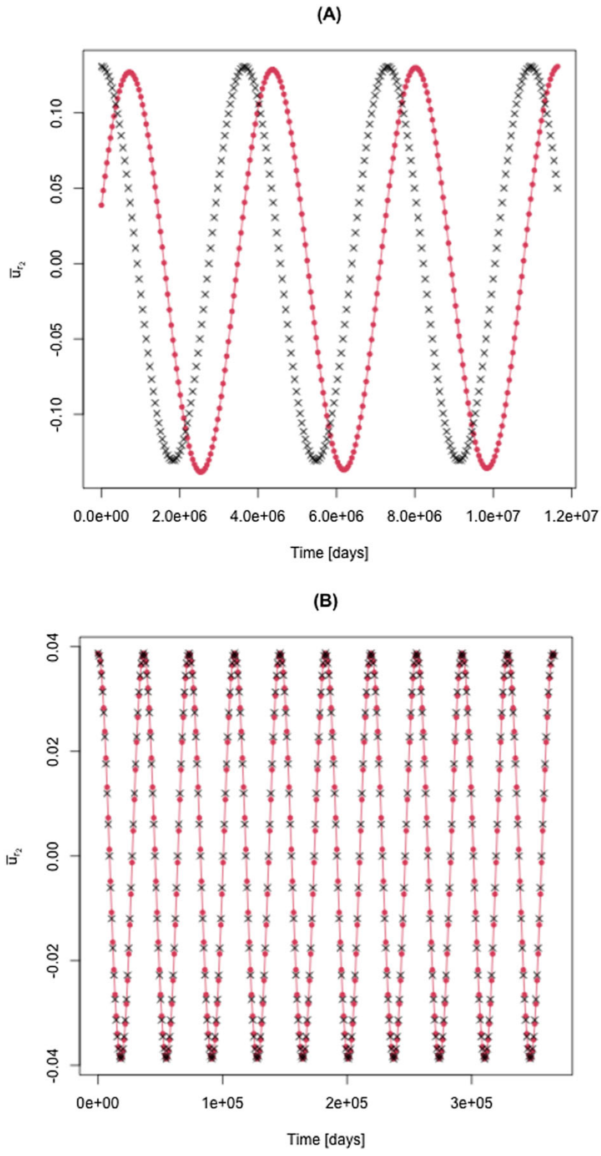

Fig. 1 Normalized surface radial displacement $\bar{u}_{r_2}$ (red dot-lines) as a function of time computed from CitcomSVE for a 2-layered Moon model and two different tidal excitation periods T: 10^4 years (**A**) and 100 years (**B**). The black cross-lines are obtained from the red lines by removing the sine contribution (see Eq. (16)). Note that $\bar{u}_{r_2}$ in red dot-line shows clear phase shift (about 70°) for T=10^4 years relative to the tidal force (the black cross-lines), but the phase shift is significantly smaller (about 2°) for the short period case. The phase shifts are controlled by the rheological structure (Table 1) and the excitation period

(2012) and Goldreich (1963), the power by the tidal forcing to a homogeneous (i.e., no core) and incompressible planetary body is given by a surface integral

$$P = \int_S \rho V_T(r_S, \theta, t) v_s \mathrm{d}s \tag{17}$$

where ρ is the density of the planet, $V_T(r_S, \theta, t)$ is the potential defined in Eq. (10) at the surface and v_s is the rate of radial displacement or radial velocity at the surface, and the integration is over the planetary surface. The radial displacement u_{r_2} can be written as Efroimsky (2012) using Eq. (8) for Love number h_2 and considering the phase shift ϵ, such

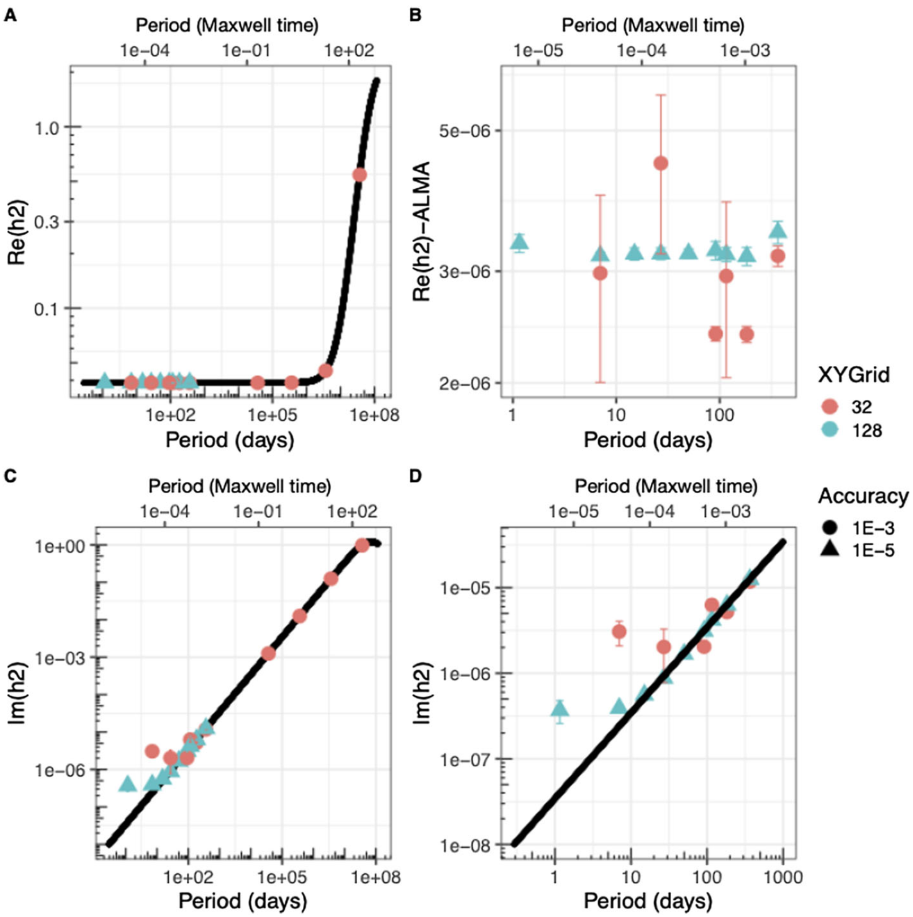

Fig. 2 The real (**A** and **B**) and imaginary (**C** and **D**) parts of Love numbers h_2 from ALMA[3] (black line) and CitcomSVE (colored points) for a 2-layered Moon model for different excitation periods, numerical resolution and accuracy. **B** is for the difference in real part of h_2 between CitcomSVE and ALMA[3] zoom-in for short periods. **D** is the zoom-in of **C** for short periods

as

$$u_{r_2} = \frac{h_2}{g} V_{T0} P_{20}(\cos\theta) \cos\left(\frac{2\pi t}{T} - \|\epsilon\|\right)$$

Considering the relationship between v_s and u_{r_2}, v_s is

$$v_s = \frac{du_{r_2}}{dt} = -\frac{h_2}{g} V_{T0} \frac{2\pi}{T} P_{20}(\cos\theta) \sin\left(\frac{2\pi t}{T} - \|\epsilon\|\right) \tag{18}$$

Substituting Eqs. (10) and (18) to Eq. (17), we can compute the power P

$$P = -\frac{4\pi}{5g} \rho h_2 V_{T0}^2 r_s^2 \frac{2\pi}{T} \sin\left(\frac{2\pi t}{T} - \|\epsilon\|\right) \cos\left(\frac{2\pi t}{T}\right). \tag{19}$$

Integrating the power P for a full period T gives us the total dissipative energy over the period,

$$\Delta E = \int_0^T P \mathrm{d}t = -\frac{4\pi^2}{5g}\rho h_2 V_{T0}^2 r_s^2 \sin\|\epsilon\|$$

where we considered $\int_0^T \frac{2\pi}{T}\sin(\frac{2\pi t}{T} - \|\epsilon\|)\cos(\frac{2\pi t}{T})\mathrm{d}t = -\pi \sin\|\epsilon\|$ (Efroimsky 2012). The quality factor is defined following Efroimsky (2012) such as $Q = \frac{1}{\sin\|\epsilon\|}$. Then, we have that the total dissipation energy over one period T is

$$\Delta E = -\frac{4\pi^2}{5g}\rho V_{T_0}^2 r_s^2 \frac{h_2}{Q} = K \times \frac{h_2}{Q} \tag{20}$$

with

$$K = -\frac{4\pi^2}{5g}\rho V_{T0}^2 r_s^2$$

For the parameters given by Table 1, $K \approx -1.47 \times 10^{17}$ joules.

Given that two quality factors Q_{ALMA} and Q_{SVE} are computed here, we will compute and compare two different dissipation energies ΔE_{ALMA} and ΔE_{SVE}, each using its corresponding h_2 and Q. It is worthwhile to point out that the power by the tidal forcing P in Eq. (17) and the total dissipative energy ΔE in Eq. (20) are for a homogeneous and incompressible planetary body without a core (Efroimsky 2012; Goldreich 1963), and that when a core is present, the work done at the core–mantle boundary (CMB) by tidal force would affect the dissipative energy (Devin and Zhong 2022).

Direct integration method The total dissipation power for the lunar mantle at different time can be computed directly from CitcomSVE (e.g., Devin and Zhong 2022) using

$$P_{\text{SVE-I}} = \int_V \frac{\tau_{ij}\tau_{ij}}{2\eta}\mathrm{d}V \tag{21}$$

where τ_{ij} is the deviatoric stress tensor, η is the viscosity, and the volume integral is for the whole computational domain or the lunar mantle. Because a CitcomSVE run is computed for multiple periods, we can calculate the total dissipative energy per period $\Delta E_{\text{SVE-I}}$ by averaging $P_{\text{SVE-I}}$ from time mT to nT as

$$\Delta E_{\text{SVE-I}} = \frac{1}{n-m}\int_{mT}^{nT} P_{\text{SVE-I}}\,\mathrm{d}t \tag{22}$$

where T is the forcing period, m and n are integers chosen for reducing the numerical error in the integral computation. In our case, we use $m = 2$ and $n = 5$.

The total dissipation energy per period from CitcomSVE $\Delta E_{\text{SVE-I}}$ can then be compared with ΔE_{SVE} and ΔE_{ALMA} from Eq. (20) derived from using the energy balance but ignoring the work done at the CMB. It should be noted that the direct integration for computing dissipation energy was also used in semi-analytical solution (Roberts and Nimmo 2008) and other numerical solution methods (Hanyk et al. 2005).

3 Results of the comparisons

Previous methods of computation are valid for gravitational k, radial h and tangential l Love numbers. As we are mainly focusing on degree-2 deformation and as k_2 and h_2 present very similar behaviors, we limit the presentation of the results to only h_2.

Table 2 Grid setup for CitcomSVE

Grid	# elements $X \times Y \times Z$	XY resolution km^2	Z resolution km	Accuracy	Time mn
Low-res	$32 \times 32 \times 128$	3085	13	1×10^{-3}	66
				1×10^{-5}	78
High-res	$128 \times 128 \times 128$	192	13	1×10^{-3}	120
				1×10^{-5}	300

Columns 3 and 4 give the resolution in km^2 in X and Y directions and in km in Z radial direction. The last column gives the execution time for a 2-layered Moon, with an excitation period of 27 days and for each configuration of numerical accuracies given in Column 5. The execution took place on 12 nodes (192 processors) with Dual Intel Xeon Gold 6248 at 2.5GHz

3.1 2-Layered Moon

Table 1 presents the main characteristics of the 2-layered Moon (i.e., the mantle and the core) considered for these tests.

The mantle is considered as a viscoelastic Maxwell material with uniform viscosity and shear modulus, and the core is a fluid. Note that in CitcomSVE calculations, the core is not explicitly included, although the core–mantle boundary is considered as described in Eq. (5).

Comparatively, in ALMA, the core properties are considered. Furthermore, as in CitcomSVE, the mantle is divided into a large number of finite elements, it is important to have a significant number of nodes for using the appropriate spatial resolution. Figure 2 gives an example of the effect of the spatial resolution on Love number h_2. Two setups are considered. The first one runs on 192 processors with a grid of $128 \times 128 \times 128$ elements (indicated with XYGrid $= 128$ in Fig. 2 or high-res in the rest of the text) for each of the 12 caps. A second setup (marked as XYGrid $= 32$ on Fig. 2 or low-res grid in the rest of the text) uses also 192 processors but with a grid of $32 \times 32 \times 128$ elements for each of the 12 caps. The advantages of the second setup are to speed up the calculation with coarser grids in horizontal directions. High-res computations were performed only when low-res appear to be not efficient enough. Table 2 lists the characteristics of the two grids (high-res and low-res) together with execution times for each configuration. A factor of almost 5 difference in the execution times exists between the lowest and highest space resolution and numerical accuracy.

Another important parameter of the simulations is the accuracy level of the solution of the governing equations given in Column 5 of Table 2. It represents the tolerance level for iterative solution procedure in the CitcomSVE solver. The smaller the parameter, the more accurate the solution is. This numerical accuracy can be tuned in CitcomSVE and in our calculations here, it varies from 10^{-3} to 10^{-5}. Finally, as explained in Sec 2.3.1, the resolution in time is also an important factor that has to be accounted for the CitcomSVE computation. A trade-off between Δt, the time increment and N, the number of time steps per period T has to be found in order to have a finer enough time resolution for the considered tidal period but also a limited propagation of the numerical error in CitcomSVE computation and for the conversion between time-dependent Love numbers to frequency-dependent imaginary and real Love numbers (see Sect. 2.3.2).

In Fig. 2, one can see the global behaviors of the imaginary and real parts of h_2 compared to ALMA^3 solutions for the two grid setups and two accuracies, and Fig. 3 gives the relative differences in percentage between CitcomSVE and ALMA^3. The error bars plotted in Fig. 2

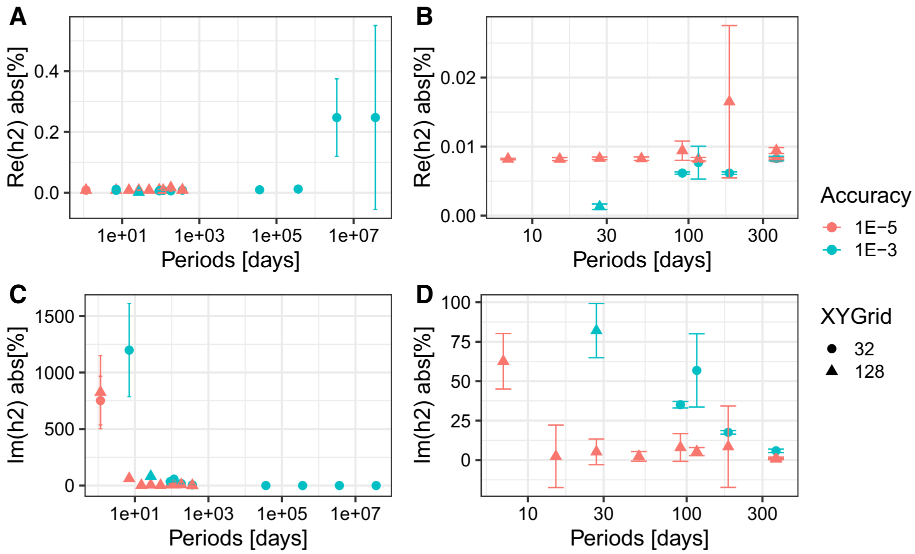

Fig. 3 Relative differences in the real and imaginary parts of h_2 between CitcomSVE and ALMA^3 for the 2-layered Moon model and for different excitation periods, numerical resolution and accuracy. **A** and **B** (resp. **C** and **D**) present the differences in real part (resp. imaginary part). **B** (resp. **D**) is a zoom-in of **A** (resp. **C**)

are uncertainties of the least square fit of the cos and sin terms of Eq. (16) for, respectively, the real and the imaginary parts of Love numbers. For the real part, with both grid setups and accuracies, the difference in h_2 between ALMA^3 and CitcomSVE is far below ($< 5 \times 10^{-6}$) the accepted differences between Love numbers deduced from different modelings (i.e., Saliby et al. (2023) and Spada (2008) for discussion). One can also notice that (i) the error bars are larger for the second setup in comparison with the first one, clearly indicating an increase in the numerical noise with the decrease in grid resolution, and (ii) these very low differences are obtained for a wide range of excitation periods (from 1 to 3×10^7 days).

For the same large range of excitation periods, the imaginary part (or the phase shift) also varies by 7 orders of magnitude (from -4×10^{-7} down to -0.97) and CitcomSVE reproduces also well the results of ALMA^3 for nearly all the cases (see Figs. 2 and 3). Imaginary parts appear to be, however, more affected by the spatial resolution and accuracy with an increase in the differences between CitcomSVE and ALMA^3 for periods of excitation smaller than 10 days. On the one hand, the impact of the spatial resolution is clearly visible in particular in Fig. 2D, where the drift between values obtained with the lowest and the highest spatial resolutions increases significantly. On the other hand, the impact of the accuracy is illustrated in Fig. 3B for example with the 27-day excitation periods for which the use of the 10^{-5} accuracy induces a decrease of the differences by a factor 8. More generally, the differences between CitcomSVE and ALMA^3 imaginary parts can be explained by the small amplitudes of the imaginary part, especially for periods of excitation below 10 days (with $Im(h_2) < 10^{-6}$) that make them more sensitive to numerical noise. For a 1-day period, the differences are greater than 50%, even in considering the highest spatial resolution and accuracy. For tidal periods greater than 10 days, the differences between ALMA^3 and CitcomSVE imaginary h_2 are below 10% (see Fig. 3) for the highest spatial resolution and accuracy and are compatible with a null difference when one accounts for the error bars of the method (see Sect. 2.3.2). In the opposite, for the low-res grid and with the lowest accuracy,

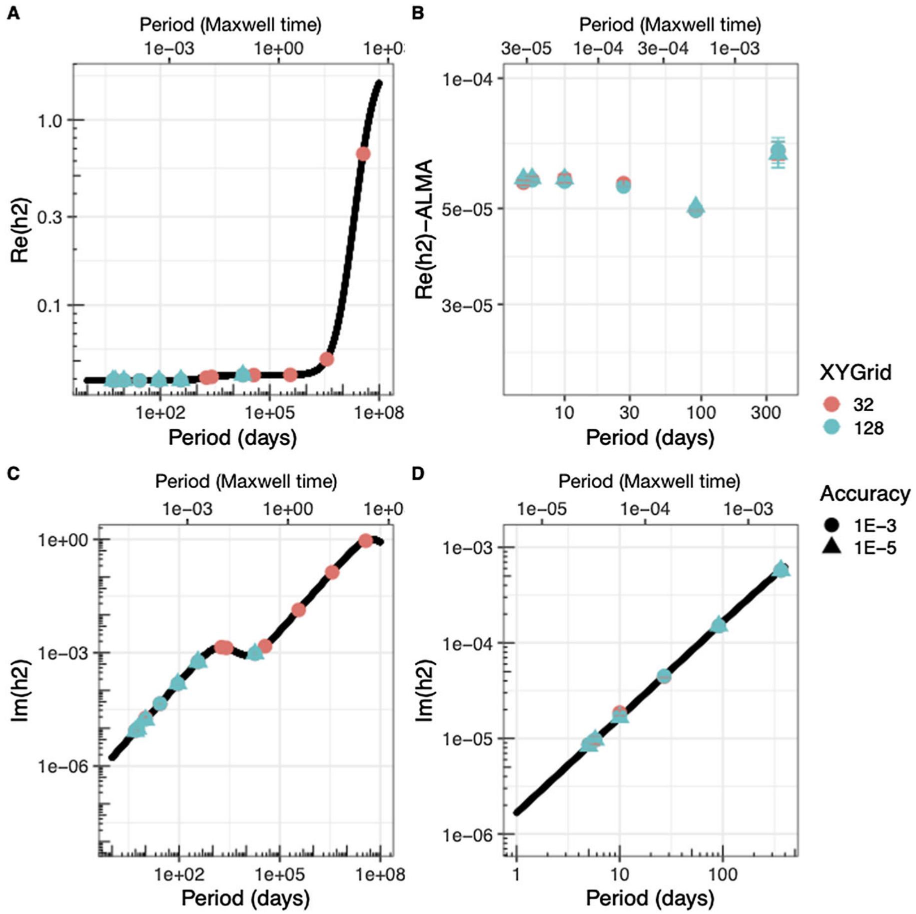

Fig. 4 Comparisons between Love numbers (h_2) obtained with ALMA[3] (black line) and CitcomSVE (colored points). Same as Fig. 2 but for the 4-layered Moon model

the differences remain greater than 10% for periods smaller than 1 year but decrease with the periods. This result shows that for periods of excitation between 1 day and 1 year, to reach a good accuracy, high spatial resolutions and accuracies are requested for this 2-layer model with mantle Maxwell time of 484 years. It is interesting to note that in the case of a 4-layered body (see Sect. 3.2), this issue is less stringent as the imaginary parts of Love numbers are bigger and less affected by numerical noise.

3.2 4-Layered Moon

From the 2-layered Moon presented in Table 1, we add two additional layers: a 38-km-thick crust with viscosity of 10^{24} Pa s located at the top of the mantle and a 119-km-thick low viscosity zone located above the fluid core, with a viscosity of 10^{18} Pa s. The shear modulus is constant for all the layers and equal to 6.56×10^{10} Pa as well as the density (3300 kg m^{-3}) except for the core (6000 kg m^{-3}). Figures 4 and 5 give, respectively, the global trend and

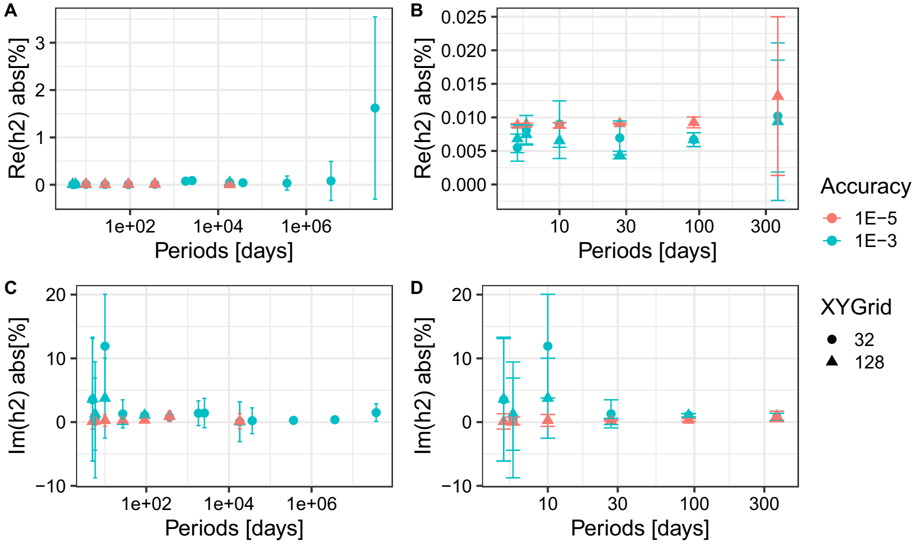

Fig. 5 Relative differences in absolute value and percentage for the real and imaginary parts of h_2 between CitcomSVE and ALMA^3 for the 4-layered Moon model and for different excitation periods, numerical resolution and accuracy. **A** and **B** (resp. **C** and **D**) present the differences in real part (resp. imaginary part). **B** (resp. **D**) is a zoom-in of **A** (resp. **C**)

the differences in percentages between CitcomSVE h_2 imaginary and real parts and ALMA^3 values for different periods of excitation in days. Same results are obtained for k_2.

The newly obtained differences between CitcomSVE and ALMA^3 are smaller than those computed for the 2-layered Moon mainly because the viscous response is now larger. This is due to the reduced viscosity for the layer above the core which induces larger dissipation and larger values in the imaginary part of Love numbers. Indeed, in Fig. 2, for a tidal period of 10 days, the imaginary Love number is of about 5×10^{-7}, whereas for the 4-layered case, the imaginary Love number is almost 2 order of magnitude larger (about 1×10^{-5}). This gain of amplitude of the phase shift explains the improved accuracy in the numerical solutions of the imaginary parts of Love numbers and the smaller differences between CitcomSVE and ALMA^3 results as one can see in Fig. 5. Even for periods smaller than 10 days, the differences remain smaller than 5% for high-resolution calculations with no significant bias. Again, the spatial resolution also plays an important role as it appears in Fig. 5. For example, for the 10-day excitation period, the use of the high-res grid reduces the differences by a factor 3 (from 12% down to 4%) and the increase in the numerical accuracy level of CitcomSVE from 10^{-3} to 10^{-5} reduces further the differences from 4 to less than 1%. This is true for all periods and, at the end, all considered periods of excitation (from 5 to 10^7 days), the differences between CitcomSVE and ALMA^3 remain below 1% for both real and imaginary parts when one uses the high-res grid and 10^{-5} for the numerical accuracy.

The Moon h_2 is estimated from Lunar Laser Ranging (LLR) observations (Williams and Boggs 2015; Viswanathan et al. 2019) and satellite altimetry measurements using the Lunar Orbiter Laser Altimeter (LOLA) onboard the Lunar Reconnaissance Orbiter (LRO, e.g., Mazarico et al. 2014; Thor et al. 2021). The derived h_2 value is 0.04394 ± 0.0002 (0.5%) and 0.0386 ± 0.0022 (5.7%), respectively, using LLR and LOLA (Viswanathan et al. 2018; Thor et al. 2021). The resulting difference between LLR and LRO estimates

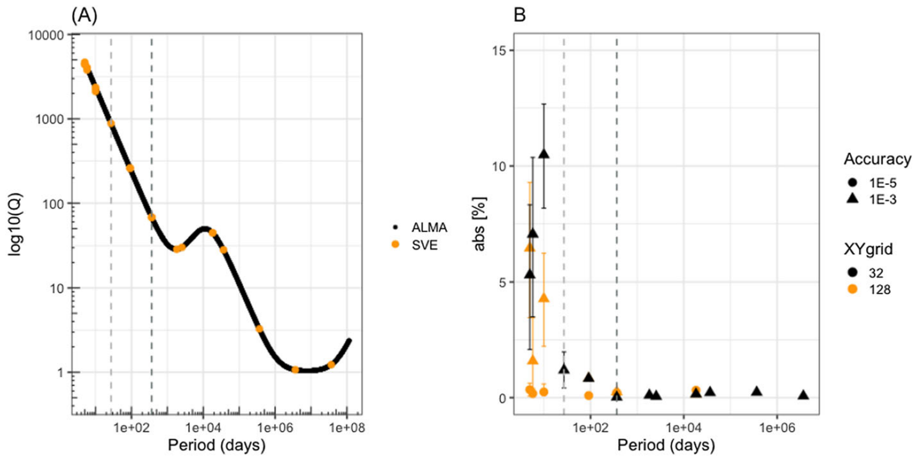

Fig. 6 **A** Comparisons between Q_{SVE} (orange circles) and Q_{ALMA} (black) for different excitation periods. **B** Relative differences in percentages and absolute values between Q_{SVE} (orange circles) and Q_{ALMA} for different excitation periods, accuracy and spatial resolutions. Both plots are for the 4-layered Moon model. The light dashed line indicates the 27 days period and the dark dashed indicates the yearly period

is therefore 0.00534 ± 0.0024 that is $12.2 \pm 5.5\%$ of the LLR estimated value. The k_2 for the Moon is mainly derived from the GRAIL mission or LLR observations within the range 0.0227–0.0310 (Williams et al. 2005, 2014). It is interesting to stress that the monthly forcing term being the most important in amplitude (Williams and Boggs 2015), most of the observed tidal signature corresponds to this monthly period (Hu et al. 2023). This means that the Love number estimations deduced from observations give mainly the amplitude of the monthly term. Consequently, the differences between Love numbers estimated numerically with CitcomSVE and ALMA^3 at the monthly period (27 days) are lower than the uncertainties of Love numbers estimated from observations.

3.3 Dissipation energy for the 4-layered Moon

In Sect. 2.3.3, we have seen that we can compute the total dissipation energy in the mantle over a period ΔE using two different methods: (i) the Q-based method in Eq. (20) and (ii) the direct integration for the mantle in Eq. (21) and (22). With the Q-based method, we may compute ΔE_{ALMA} and ΔE_{SVE} using Q_{ALMA} and Q_{SVE}, respectively. The second method is only applicable to CitcomSVE calculations and computes $\Delta E_{\mathrm{SVE\text{-}I}}$.

By comparing Q_{ALMA} and Q_{SVE}, we assess the differences between CitcomSVE and ALMA^3 in using the same assumption of incompressible and homogeneous planetary body with no core in the computation of the tidal dissipation energy. The result of this comparison should be similar to the comparisons of Love numbers h_2 between CitcomSVE and ALMA^3 (see Fig. 5). It is indeed what one can see in Fig. 6 where a good agreement is evident both in the global behavior of Q_{ALMA} and Q_{SVE} (Fig. 6A) and in the relative differences between them (Fig. 6B). As for the imaginary parts, the main differences occur for short periods (smaller than 1 year). In this case, the numerical accuracy used for solving the governing equations with CitcomSVE plays a major role. The agreement between Q_{ALMA} and Q_{SVE} is better than 1% for all the periods considered with high spatial resolutions and numerical accuracy. For periods greater than 1 year, even with low resolutions and accuracy the differences remain

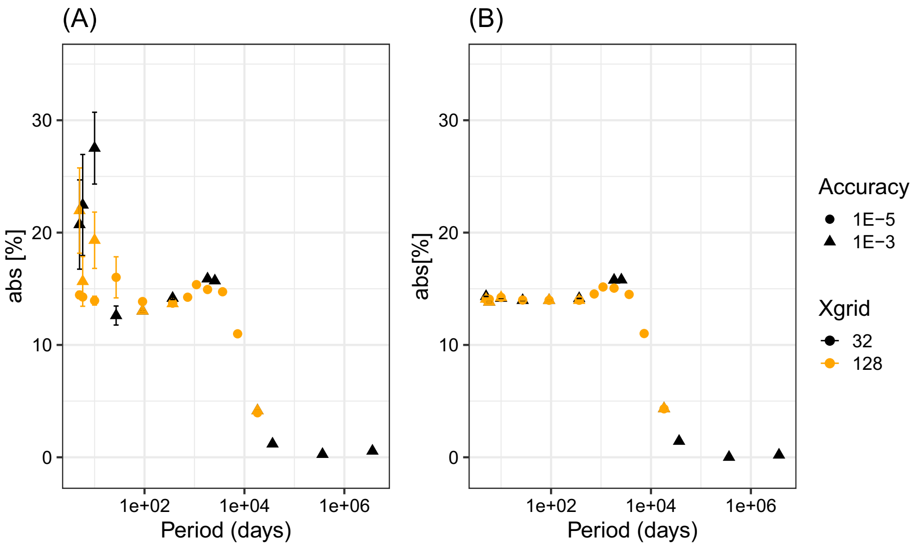

Fig. 7 Relative differences in percentages and absolute values between $\Delta E_{\text{SVE-I}}$ and ΔE_{SVE} (**A**) and between $\Delta E_{\text{SVE-I}}$ and ΔE_{ALMA} (**B**) for the 4-layered Moon and for different excitation periods, accuracy and spatial resolutions

smaller than 1%. We stress that because Q is defined by surface radial displacement Love number h_2 (see Eq. (15)), the excellent agreement between Q_{ALMA} and Q_{SVE} indicates the agreement in Love number h_2 from CitcomSVE and ALMA[3].

Now let us investigate dissipation energy over one period by considering three different formulations: ΔE_{ALMA}, ΔE_{SVE}, and $\Delta E_{\text{SVE-I}}$. Again, while the first two Q-based $\Delta E's$ ignore the effects of the CMB, $\Delta E_{\text{SVE-I}}$ includes the CMB's contribution. The differences between $\Delta E_{\text{SVE-I}}$ and ΔE_{SVE}, plotted in Fig. 7, would indicate the possible effects of the CMB on dissipation energy and also how the Q-based approach may differ from the full integral of the work and consequently from the total energy dissipation. For periods greater than 5 years, there is a good agreement between the two quantities with relative differences smaller than 5%. For periods smaller than 5 years, an average difference of about 14% is present with more numerical noise for periods smaller than 3 months. In this case, as with Fig. 6, a numerical accuracy of about 10^{-5} is required. The differences between $\Delta E_{\text{SVE-I}}$ and ΔE_{ALMA} are plotted in Fig. 7B. As expected, they follow the same trends as in Fig. 7A but with less noise for smaller than 3-month periods for all accuracies and resolutions. This stresses the very good numerical accuracy of the $\Delta E_{\text{SVE-I}}$ which appears to be less sensitive to numerical accuracy than ΔE_{SVE}.

For both comparisons, relative differences of about 14% between the Q-based ΔE and $\Delta E_{\text{SVE-I}}$ exist for periods smaller than 5 years. One possible explanation is the impact of the CMB as it has been shown (Briaud et al. 2023b) that a fluid Newtonian core with or without an elastic inner core may affect the dissipation more at short periods, while at longer periods the dissipation is more sensitive to the mantle.

4 Conclusion

In this work, we have presented the first results obtained in using the finite element solutions of the governing equations in the case of periodic tidal excitations using the software CitcomSVE. Comparisons with semi-analytical methods and the software ALMA[3] (Melini et al. 2022) were done in using the formalism of the complex frequency-dependent Love numbers and for two different 1-D Moon viscoelastic profiles (a 2-layered body and a 4-layered body).

For the vast majority of the profiles, they show very good agreement between the finite element and the semi-analytical solutions. For short periods (less than 7 days) and for a 2-layered body with an uniform mantle, the differences can be large since the imaginary part of Love numbers is small. But, by using optimal space and time resolutions, the differences can be significantly reduced. The spatial resolution and the numerical accuracy are then important for obtaining the best agreement with semi-analytical solutions. For the 4-layered Moon, with a 12×128^3 spatial resolution and 10^{-5} accuracy, the differences for real and imaginary parts of Love numbers between CitcomSVE and semi-analytical solutions are below 1% for periods of excitation from 5 to 10^8 days.

We also estimated the total dissipation energies with the quality factor Q approach (Efroimsky 2012), ΔE_{ALMA} and ΔE_{SVE}, and with the formalism proposed by Devin and Zhong (2022) and implemented in CitcomSVE, $\Delta E_{\text{SVE-I}}$. Comparisons indicate that $\Delta E_{\text{SVE-I}}$ is less noisy than the Q-basedΔE_{SVE}.This is consistent with the numerical uncertainties identified in the frequency-dependent Love numbers decomposition presented in Sect. 2.3.2 and discussed in Sect. 3.1.

Furthermore, we note a difference of about 14 % between $\Delta E_{\text{SVE-I}}$ and Q-based ΔE_{ALMA} for excitation periods smaller than 10^4 days. The main difference in their defining equations is the dissipation energy associated with the deformation of the CMB—accounted for in $\Delta E_{\text{SVE-I}}$ but not in ΔE_{SVE} or in ΔE_{ALMA}—suggesting that the influence of the core contribution needs to be more better accounted for in the Q-based method. Based on these results, it would be interesting to continue these comparisons for icy satellites for which the contribution of the core is supposed to be more important than in the case of the Moon.

Acknowledgements This work was supported by the French government, through the UCAJEDI Investments in the Future project managed by the National Research Agency (ANR) under Reference No. ANR-15-IDEX-01. The authors are grateful to the OPAL infrastructure and the Université Côte d'Azur Center for High-Performance Computing for providing resources and support. SJZ's work is supported by Grants US-NSF EAR-2222115 and NASA 80NSSC23M0161. AB was supported by the European Research Council (ERC) under the European Union's Horizon 2020 research and innovation program (Advanced Grant AstroGeo-885250).

References

Boughanemi, A., Mémin, A.: Effects of andrade and burgers rheologies on glacial isostatic adjustment modeling in Antarctica. Geod. Geodyn. (2024). https://doi.org/10.1016/j.geog.2023.12.008

Briaud, A., Ganino, C., Fienga, A., Mémin, A., Rambaux, N.: The lunar solid inner core and the mantle overturn. Nature **617**(7962), 743–746 (2023a). https://doi.org/10.1038/s41586-023-05935-7

Briaud, A., Fienga, A., Melini, D., Rambaux, N., Mémin, A., Spada, G., Saliby, C., Hussmann, H., Stark, A., Viswanathan, V., Baguet, D.: Constraints on the lunar core viscosity from tidal deformation. Icarus **394**, 115426 (2023b). https://doi.org/10.1016/j.icarus.2023.115426. arXiv:2301.04035 [astro-ph.EP]

Broquet, A., Andrews-Hanna, J.C.: Geophysical evidence for an active mantle plume underneath Elysium Planitia on Mars. Nat. Astron. **7**, 160–169 (2023). https://doi.org/10.1038/s41550-022-01836-3

Devin, E., Zhong, S.: Characterization of viscous dissipative heating in the Earth's mantle caused by surface forces. Geochem. Geophys. Geosyst. **23**(10), 2021–010218 (2022). https://doi.org/10.1029/2021GC010218
Duncombe, J.: The unsolved mystery of the earth blobs. Eos (2019). https://doi.org/10.1029/2019EO117193
Efroimsky, M.: Bodily tides near spin-orbit resonances. Celest. Mech. Dyn. Astron. **112**(3), 283–330 (2012). https://doi.org/10.1007/s10569-011-9397-4. arXiv:1105.6086 [astro-ph.EP]
French, S.W., Romanowicz, B.A.: Broad plumes rooted at the base of the Earth's mantle beneath major hotspots. Nature **525**, 95–99 (2015)
Ge-Ruo, A., Wahr, J., Zhong, S.: Computations of the viscoelastic response of a 3-D compressible Earth to surface loading: an application to Glacial Isostatic Adjustment in Antarctica and Canada. Geophys. J. Int. **192**(2), 557–572 (2013). https://doi.org/10.1093/gji/ggs030
Goldreich, P.: On the eccentricity of satellite orbits in the solar system. Mon. Notices R. Astron. Soc. **126**, 257–268 (1963). https://doi.org/10.1093/mnras/126.3.257
Hanyk, V., Matyska, C., Yuen, D.A.: Short time-scale heating of the Earth's mantle by ice-sheet dynamics. Earth Planets Space **57**(9), 895–902 (2005). https://doi.org/10.1186/bf03351867
Harada, Y., Goossens, S., Matsumoto, K., Yan, J., Ping, J., Noda, H., Haruyama, J.: Strong tidal heating in an ultralow-viscosity zone at the core-mantle boundary of the moon. Nat. Geosci. **7**(8), 569–572 (2014)
Harder, H., Christensen, U.R.: A one-plume model of Martian mantle convection. Nature **380**, 507–509 (1996)
Hu, X., Stark, A., Dirkx, D., Hussmann, H., Fienga, A., Briaud, A., Mémin, A., Melini, D., Fayolle, M., Rambaux, N., Baguet, D., Oberst, J.: Sensitivity analysis of polar orbiter motion to lunar viscoelastic tidal deformation. Celest. Mech. Dyn. Astron. **135**(2), 16 (2023). https://doi.org/10.1007/s10569-023-10131-w
Kang, K., Zhong, S., Ge-Ruo, A., Mao, W.: The effects of non-Newtonian rheology in the upper mantle on relative sea level change and geodetic observables induced by glacial isostatic adjustment process. Geophys. J. Int. **228**(3), 1887–1906 (2022). https://doi.org/10.1093/gji/ggab428
Klemann, V., Martinec, Z., Ivins, E.R.: Glacial isostasy and plate motion. J. Geodyn. **46**(3), 95–103 (2008). https://doi.org/10.1016/j.jog.2008.04.005
Latychev, K., Mitrovica, J.X., Tromp, J., Tamisiea, M.E., Komatitsch, D., Christara, C.C.: Glacial isostatic adjustment on 3-D earth models: a finite-volume formulation. Geophys. J. Int. **161**, 421–444 (2005). https://doi.org/10.1111/j.1365-246x.2005.02536.x
Lau, H.C.P., Mitrovica, J.X., Davis, J.L., Tromp, J., Yang, H.-Y., Al-Attar, D.: Tidal tomography constrains earth's deep-mantle buoyancy. Nature **551**(7680), 321–326 (2017). https://doi.org/10.1038/nature24452
Maguire, R., Ritsema, J., Bonnin, M., Keken, P.E., Goes, S.: Evaluating the resolution of deep mantle plumes in teleseismic traveltime tomography. J. Geophys. Res. Solid Earth **123**(1), 384–400 (2018). https://doi.org/10.1002/2017JB014730
Mazarico, E., Barker, M.K., Neumann, G.A., Zuber, M.T., Smith, D.E.: Detection of the lunar body tide by the Lunar Orbiter Laser Altimeter. Geophys. Res. Lett. **41**, 2282–2288 (2014). https://doi.org/10.1002/2013GL059085
Melini, D., Saliby, C., Spada, G.: On computing viscoelastic Love numbers for general planetary models: the ALMA^3 code. Geophys. J. Int. **231**(3), 1502–1517 (2022). https://doi.org/10.1093/gji/ggac263
Murray, C.D., Dermott, S.F.: Solar System Dynamics (2000). https://doi.org/10.1017/CBO9781139174817
Paulson, A., Zhong, S., Wahr, J.: Modelling post-glacial rebound with lateral viscosity variations. Geophys. J. Int. **163**(1), 357–371 (2005). https://doi.org/10.1111/j.1365-246X.2005.02645.x
Qin, C., Zhong, S., Wahr, J.: A perturbation method and its application: elastic tidal response of a laterally heterogeneous planet. Geophys. J. Int. **199**(2), 631–647 (2014). https://doi.org/10.1093/gji/ggu279
Ritsema, J., Deuss, A., Van Heijst, J.H., Woodhouse, J.H.: S40RTS: a degree-40 shear-velocity model for the mantle from new Rayleigh wave dispersion, teleseismic traveltime and normal-mode splitting function measurements. Geophys. J. Int. **184**, 1223–1236 (2011)
Roberts, J.H., Nimmo, F.: Tidal heating and the long-term stability of a subsurface ocean on Enceladus. Icarus **194**(2), 675–689 (2008). https://doi.org/10.1016/j.icarus.2007.11.010
Saliby, C., Fienga, A., Briaud, A., Mémin, A., Herrera, C.: Viscosity contrasts in the Venus mantle from tidal deformations. Planet. Space Sci. **231**, 105677 (2023). https://doi.org/10.1016/j.pss.2023.105677. arXiv:2305.02278 [astro-ph.EP]
Spada, G.: Alma, a fortran program for computing the viscoelastic love numbers of a spherically symmetric planet. Comput. Geosci. **34**(6), 667–687 (2008)
Spada, G.: A benchmark study for glacial isostatic adjustment codes. Geophys. J. Int. **185**(1), 106–132 (2011)
Spada, G., Boschi, L.: Using the post-widder formula to compute the earth's viscoelastic love numbers. Geophys. J. Int. **166**(1), 309–321 (2006)
Tan, Y., Harada, Y.: Tidal constraints on the low-viscosity zone of the moon. Icarus **365**, 114361 (2021)

Thor, R., Kallenbach, R., Christensen, U., Gläser, P., Stark, A., Steinbrügge, G., Oberst, J.: Determination of the lunar body tide from global laser altimetry data. J. Geod. (2021). https://doi.org/10.1007/s00190-020-01455-8
van der Wal, W., Barnhoorn, A., Stocchi, P., Gradmann, S., Wu, P., Drury, M., Vermeersen, B.: Glacial isostatic adjustment model with composite 3-D Earth rheology for Fennoscandia. Geophys. J. Int. **194**(1), 61–77 (2013)
Viswanathan, V., Fienga, A., Minazzoli, O., Bernus, L., Laskar, J., Gastineau, M.: The new lunar ephemeris inpop17a and its application to fundamental physics. Mon. Not. R. Astron. Soc. **476**(2), 1877–1888 (2018). https://doi.org/10.1093/mnras/sty096. arXiv:1710.09167 [gr-qc]
Viswanathan, V., Rambaux, N., Fienga, A., Laskar, J., Gastineau, M.: Observational constraint on the radius and oblateness of the lunar core-mantle boundary. Geophys. Res. Lett. **46**(13), 7295–7303 (2019)
Wahr, J., Selvans, Z.A., Mullen, M.E., Barr, A.C., Collins, G.C., Selvans, M.M., Pappalardo, R.T.: Modeling stresses on satellites due to nonsynchronous rotation and orbital eccentricity using gravitational potential theory. Icarus **200**(1), 188–206 (2009). https://doi.org/10.1016/j.icarus.2008.11.002
Wieczorek, M., Neumann, G., Nimmo, F., Kiefer, W., Taylor, G., Melosh, R.J.H., Solomon, S., Andrews-Hanna, J., Asmar, S.: The crust of the moon as seen by grail. Science **339**(6120), 671–675 (2013)
Williams, J.G., Boggs, D.H.: Tides on the moon: theory and determination of dissipation. J. Geophys. Res. Planets **120**(4), 689–724 (2015)
Williams, J., Boggs, D., Ratcliff, J.: Lunar fluid core and solid-body tides. Lunar and Planetary Science XXXVI, Part 21 (2005)
Williams, J., Konopliv, A., Boggs, D., Park, R., Yuan, D., Lemoine, F., Goossens, S., Mazarico, E., Nimmo, F., Weber, R., Asmar, S., Jay Melosh, H., Neumann, G., Phillips, R., Smith, D., Solomon, S., Watkins, M., Wieczorek, M., Andrews-Hanna, J., Head, J., Kiefer, W., Matsuyama, I., McGovern, P., Jeffrey Taylor, G., Zuber, M.: Lunar interior properties from the GRAIL mission. J. Geophys. Res. Planets **119**(7), 1546–1578 (2014). https://doi.org/10.1002/2013JE004559
Zhong, S.: Migration of Tharsis volcanism on Mars caused by differential rotation of lithosphere. Nat. Geosci. **2**, 19–23 (2009). https://doi.org/10.1038/NGEO392
Zhong, S., Zuber, M.T., Moresi, L., Gurnis, M.: Role of temperature-dependent viscosity and surface plates in spherical shell models of mantle convection. J. Geophys. Lett. **105**(B5), 11063–11082 (2000). https://doi.org/10.1029/2000JB900003
Zhong, S., Paulson, A., Wahr, J.: Three-dimensional finite-element modelling of Earth's viscoelastic deformation: effects of lateral variations in lithospheric thickness. Geophys. J. Int. **155**(2), 679–695 (2003). https://doi.org/10.1046/j.1365-246X.2003.02084.x
Zhong, S., McNamara, A., Tan, E., Moresi, L., Gurnis, M.: A benchmark study on mantle convection in a 3-D spherical shell using CitcomS. Geochem. Geophys. Geosyst. **9**(10), 10017 (2008). https://doi.org/10.1029/2008GC002048
Zhong, S., Qin, C., Ge-Ruo, A., Wahr, J.: Can tidal tomography be used to unravel the long-wavelength structure of the lunar interior? Geophys. Res. Lett. **39**(15), 15201 (2012). https://doi.org/10.1029/2012GL052362
Zhong, S., Kang, K., Ge-Ruo, A., Qin, C.: CitcomSVE: a three-dimensional finite element software package for modeling planetary Mantle's viscoelastic deformation in response to surface and tidal loads. Geochem. Geophys. Geosyst. **23**(10), 2022–010359 (2022). https://doi.org/10.1029/2022GC010359